REMARKS

Claims 1-12, 23-40, 42-44 and 46-49 are pending in this application. The Office Action rejects claims 13-15, 18 and 36 under 35 U.S.C. §102(b); and rejects claims 16, 17, 19-34, 37, 38, 40-48 and 50 under 35 U.S.C. §103(a). By this amendment, claims 13-22, 36-38, 41, 45 and 50 are canceled.

Applicant appreciates the courtesies extended by Examiner Chuo to Applicant's representative during the personal interview conducted on December 20, 2006. Applicant's separate record of the substance of the personal interview is incorporated into the Remarks below.

Entry of the amendments is proper under 37 CFR §1.116 since the amendments: (a) place the application in condition for allowance for the reasons discussed herein; (b) do not raise any new issue requiring further search and/or consideration as the amendments amplify issues previously discussed throughout prosecution; (c) satisfy a requirement of form asserted in the previous Office Action; (d) do not present any additional claims without canceling a corresponding number of finally rejected claims; and (e) place the application in better form for appeal, should an appeal be necessary. The amendments are necessary and were not earlier presented because e.g. they are made in response to arguments raised in the final rejection. Entry of the amendments is thus respectfully requested.

I.   Rejection Under 35 U.S.C. §102(b)

The Office Action rejects claims 13-15, 18 and 36 under 35 U.S.C. §102(b) as being anticipated by Edlund (JP 07-185277; hereafter "Edlund"). The Office Action asserts that Edlund teaches a substrate formed from vanadium, an inorganic electrolyte layer formed on both sides of the substrate and a hydrogen permeable coating layer.

Applicants cancel claims 13-15, 18 and 36 in order to obviate the rejection.

For at least the foregoing reason, this rejection is moot. Reconsideration and withdrawal of the rejection are earnestly solicited.

II. Rejections Under 35 U.S.C. §103(a)

A. Rejection of claims 16 and 17 over Edlund in view of Hockaday (US 5759712; hereafter "Hockaday"); claims 19 and 20 over Edlund in view of Hara (US 2003/0044667; hereafter "Hara"); and claims 21-22, 37 and 38 over Edlund in view of Vaughey et al. (US 6,521,202; hereafter "Vaughey"); and claims 41-42, 45-46 and 50 over Edlund in view of Smotkin.

The Office Action rejects claims 16 and 17 under 35 U.S.C. §103(a) as being unpatentable over Edlund in view of Hockaday; rejects claims 19 and 20 under 35 U.S.C. §103(a) as being unpatentable over Edlund in view of Hara; rejects claims 21-22, 37 and 38 under 35 U.S.C. §103(a) as being unpatentable over Edlund in view of Vaughey; and rejects claims 41-42, 45-46 and 50 over Edlund in view of Smotkin.

Applicants hereby cancel claims 16-17, 19-22, 37-38, 41-42, 45-46 and 50; thus, these rejections are moot.

Reconsideration and withdrawal of the rejections are earnestly solicited.

B. Rejection of claims 23-25, 28-30, 33-34, 43-44, 47 and 48 over Hara in view of Edlund; claims 26-27 over Hara in view of Edlund and in further View of Hockaday; and claims 31 and 32 over Hara in view of Edlund and in further view of Vaughey; and claims 43-44, 47 and 48 over Hara in View of Edlund and further in view of Smotkin.

The Office Action rejects claims 23-25, 28-31 and 33, 34, 43, 44, 47 and 48 under 35 U.S.C §103(a) as being unpatentable over Hara in view of Edlund. The Office Action asserts that Hara discloses the claimed invention except for the electrolyte membrane as disclosed by Edlund. Edlund is also cited as containing an inorganic electrolyte that is NiO. The Office Action also rejects claims 26 and 27 under 35 U.S.C. §103(a) as being unpatentable over Hara in view of Edlund and in further view of Hockaday; rejects claims 31 and 32 under 35 U.S.C. §103(a) as being unpatentable over Hara in view of Edlund and in

further view of Vaughey; and claims 43, 44, 47 and 48 over Hara in View of Edlund and in

Further view of Smotkin. Because the rejections are related, they are addressed together in the

following remarks. Applicant respectfully traverses these rejections.

The rejections are predicated on the assertion that Hara in view of Edlund teaches the

claimed hydrogen permeable material. In accordance with the recommendation of Examiner

Chuo during the personal interview conducted on December 20, 2006, Applicants submit

herewith evidence establishing that Edlund's *hydrogen permeable* membrane containing NiO

is not equivalent to an *electrolyte membrane* as claimed, which renders all instant pending

claims allowable.

Instant claims 23 and 40, and each claim depending therefrom, involve an electrolyte

membrane. In contrast, Edlund merely teaches separating hydrogen from other gases. As the

enclosed article generally confirms, NiO easily reacts with hydrogen gas to produce Ni

metal.[1] However, Ni metal has high electrical conductivity, and the generation of Ni from

NiO causes a short circuit in the electrolyte membrane layer. Thus, Edlund's hydrogen

separation membrane can work as a hydrogen separation membrane, but would not work as

an electrolyte membrane layer. For at least this reason, Hara in view of Edlund would not

have rendered obvious the claimed invention. Moreover, Hara in view of Edlund and further

in view of any of Hockaday, Vaughey or Smotkin do not remedy these deficiencies.

For at least the foregoing reasons, Hara in view of Edlund and further in view of any

of Hockaday, Vaughey or Smotkin would not have rendered obvious the claimed invention.

Reconsideration and withdrawal of the rejection are earnestly solicited.

---

[1] See attached: Richardson, et. al. "X-Ray Diffraction Study of Nickel Oxide Reduction by
Hydrogen," Applied Catalysis A: General 246 (2003) 137-150. See specifically page 141,
§2.3 Experimental Procedure; and p 143, §3.1 in which NiO reacts to form Ni metal.

III.   **Conclusion**

In view of the foregoing, it is respectfully submitted that this application is in condition for allowance. Favorable reconsideration and prompt allowance of the application are earnestly solicited.

Should the Examiner believe that anything further would be desirable in order to place this application in even better condition for allowance, the Examiner is invited to contact the undersigned at the telephone number set forth below.

Respectfully submitted,

James A. Oliff
Registration No. 27,075

Ryan C. Cady
Registration No. 56,762

JAO:RCC/hms

Attachment:
    Richardson, et. al. "X-Ray Diffraction Study of Nickel Oxide Reduction by Hydrogen," Applied Catalysis A: General 246 (2003) 137-150

Date: February 8, 2007

OLIFF & BERRIDGE, PLC
P.O. Box 19928
Alexandria, Virginia 22320
Telephone: (703) 836-6400

DEPOSIT ACCOUNT USE
AUTHORIZATION
Please grant any extension
necessary for entry;
Charge any fee due to our
Deposit Account No. 15-0461

ELSEVIER

APPLIED CATALYSIS A: GENERAL.

X-ray diffraction study of nickel oxide reduction by hydrogen

James T. Richardson [a,*], Robert Scates [a], Martyn V. Twigg [b]

[a] *Department of Chemical Engineering, University of Houston, Cullen Blvd., Houston, TX 77204-4792, USA*
[b] *Johnson Matthey, Orchard Road, Royston, Herts SG8 5HE, UK*

Abstract

Hydrogen reduction of porous bulk NiO particles has been studied with in situ hot-stage X-ray diffraction (XRD) in the temperature range 175–300 °C. This technique has the ability to measure NiO disappearance and Ni appearance simultaneously, together with the crystallite size of each. Since the sample was a very thin, 50-μm slab of dispersed 20-μm diameter grains, textural and morphological features normally encountered during studies with fixed beds of NiO particles were absent and measurements reflected only the chemical mechanism and kinetics.

The results indicated that reduction in the absence of water added to the reducing gas followed a series of steps: (1) an induction period associated with the initial reduction of NiO and the appearance of Ni metal clusters; (2) acceleration of the reduction rate as the size of the clusters increase; and (3) a pseudo-first-order (excess H_2) process in which NiO disappeared and Ni appeared in concert until reduction slowed at a fractional conversion of about 0.8. Crystallite size measurements showed NiO crystallites of about 3 nm in size were transformed into Ni crystallites of more than 20 nm, implying that Ni^0 ion transport following reduction was very fast due to the close proximity of the NiO crystallites being reduced.

When 2.2×10^{-2} atm of H_2O was added to the reducing gas, induction times increased by approximately a factor of two and reduction rates decreased (increasingly at lower temperatures) with an apparent activation energy of 126 ± 27 kJ mol^{-1} compared to 85 ± 6 kJ mol^{-1} without added water. The lag between NiO reduction and Ni growth observed in previous studies was not seen, indicating that textural and morphological factors are very important in establishing the role of water vapor in the reduction process.
© 2003 Elsevier Science B.V. All rights reserved.

Keywords: Nickel oxide reduction; In situ hot-stage X-ray diffraction

1. Introduction

Reduction of nickel oxide by H_2

$$NiO + H_2 \rightarrow Ni + H_2O \qquad (1)$$

is irreversible, since the equilibrium constant, K_p, varies from 10^3 to 10^2 in the temperature range 0–1000 °C, and the reaction is only slightly exother-

* Corresponding author. Tel.: +1-713-7434324;
fax: +1-713-7434323.
E-mail address: jtr@uh.edu (J.T. Richardson).

mic. Extensive studies on reaction (1) have appeared in the literature, due to its practical importance in the reduction of nickel ores [1] and catalysts [2]. It is also a model reaction for oxide reduction mechanisms, since only two solid phases are involved (as contrasted to iron oxide [3]) and no excessive heat effects are present (as with CuO [4]).

The first reported systematic measurements of bulk NiO reduction was by Benton and Emmett in 1924 [5]. These authors measured water formation as an indication of the extent of reaction, and their results are reproduced in Fig. 1 for a sample of NiO made
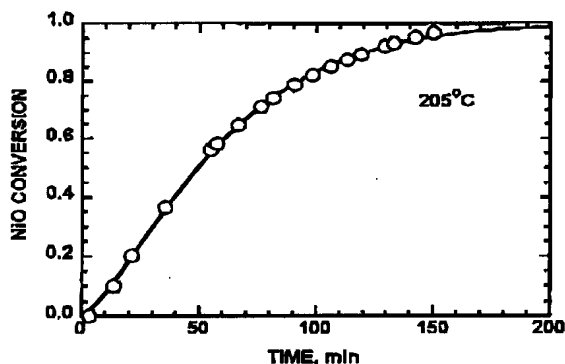
Fig. 1. NiO reduction data of Benton and Emmett [5]: NiO, 4.8 g, 205 °C.

by heating nickel nitrate at 400 °C. Their seminal research introduced many of the conclusions regarding NiO reduction that are accepted today. These are: (1) reduction occurs at the interface between NiO and previously reduced Ni; (2) there is an "autocatalytic" effect, i.e. reduction rate is proportional to the interfacial area; (3) there is an induction (i.e. nucleation) period that depends on the nature of the sample and temperature; and (4) added water reduces the reduction rate and increases the induction period. This work was confirmed in 1930 by Taylor and Starkweather [6], who measured hydrogen consumption during reduction and demonstrated the catalytic effect by adding metallic nickel to the oxide.

These early experiments were followed by numerous studies that revealed the complexity of the reduction process, and results up to 1979 were reviewed by Boldyrev et al. [7]. Among features that influence the induction period are the presence of defects or altervalent ions in the outer surface of NiO grains [8–13], thereby emphasizing the sensitivity of the initiation or nucleation process to impurities, preparational parameters and pretreatment. Even the thermomagnetic phase transition at 260 °C (the Neel temperature of antiferromagnetic NiO) produces an anomaly in reduction rate versus temperature curves [14].

Although emphasizing why experimental findings often differ from one study to another, these results also gave insight into the prevailing mechanism for chemical reduction. This is: (1) dissociation of H_2 (initially by NiO during the induction period, then by pre-

viously formed Ni metal at the growing interface); (2) surface diffusion of hydrogen atoms to a reactive center; (3) rupture of Ni–O bonds to produce Ni^0 atoms; (4) nucleation of Ni^0 atoms into metallic clusters; and (5) growth of nickel metal clusters into crystallites.

Since H_2 is often in excess, the kinetics of the overall process can be interpreted as pseudo-first-order

$$-r_{NiO} = (kP_H)C_{NiO} \qquad (2)$$

where k is the intrinsic chemical rate constant, P_H the partial pressure of H_2, and C_{NiO} is the concentration of NiO. The common practice has been to find (kP_H) from curves such as Fig. 1 by taking the slope at the point where it is most linear, usually at about 50% conversion.

Koga and Harrison, reviewed general reactions between solids and H_2 and represented the induction process as generation of nickel atoms on the outer surface of NiO grains [15]. Following nucleation, Ni clusters grow two-dimensionally across the surface until they overlap, at which point H_2 rapidly dissociates on Ni and the interface proceeds quickly into the grain. This growth of clusters is a special case of a class of solid phase mechanisms discussed in 1940 by Avrami, who developed the relationship given in Eq. (3) [16–18]:

$$x_{NiO} = 1 - \exp(-kt^m) \qquad (3)$$

where x_{NiO} is the fractional conversion at time t, k an overall rate constant, and m is an exponent whose value (0.5–4) depends on grain geometry and the limiting step (i.e. chemical nucleation or diffusion). Eq. (3) is sigmoidal in shape for low values of k and can account for many observed reduction curves. It is interesting that the curve through the points in Fig. 1 is Eq. (3) fitted to the data with $m = 1.34$, suggests three-dimensional growth and instantaneous nucleation with the rate controlled by diffusion across the interface, but there is no other evidence to support this.

Bandrowski et al. [19] measured water produced during the reduction to generate sigmoidal conversion curves they explained with a two-step kinetic model. The first step, reaction between NiO and hydrogen atoms adsorbed on NiO, predominates in the early part of the reduction and is proportional to the square root of the H_2 pressure. The second step is reaction at the metal-oxide interface between NiO and hydrogen atoms adsorbed on previously reduced NiO. This step

is independent of H_2 pressure and dominates in the final stages of reduction. Although this model fits the data above 300 °C, the authors concluded that H_2 diffusional effects occurred below 300 °C. They verified reduction retardation by added water and introduced a Langmiur–Hinshelwood adsorptive term to the rate equation:

$$-r_{NiO} = \frac{(kP_H)C_{NiO}}{1 + K_w P_w} \tag{4}$$

where P_w is the partial pressure of water vapor and K_w an adsorption coefficient. However, the Avrami model also gives just as good a fit ($m = 2.07$) for their published data at 295 °C.

These early models emphasized the chemical mechanism and kinetics of the reduction process, but there was little uniformity in the physical properties of NiO grains and pellets used. Nevertheless, it was suspected that morphological factors were just as important as topological properties in determining the course of the reduction. This was demonstrated by Moriyama and Yamaguchi [20], who found that reduction rate constants were inversely proportional to grain size above a diameter of about 10 μm [21]. Such dependence is predicted by the classical shrinking core model [22], in which the Ni–NiO interface moves towards the center of the grain, leaving behind a porous metallic product layer through which H_2 diffuses in and H_2O out. Various rate equations can be derived, depending on which process is slowest. With chemical reaction at the interface controlling, the model leads to Eq. (5):

$$x_{NiO} = 1 - (1 - k_c t)^3 \tag{5}$$

where $k_c = (kP_H)/R_g$ (R_g is the grain radius).

Delmon [23] argued that grain size dependence is consistent with nucleation at the interface. As R_g decreases, the rate increases, first according to the shrinking core model and then progressively slower, since nucleation becomes increasingly rate-limiting and k_c decreases at lower sizes. According to Delmon and Pouchot [24], the limiting value for uniform behavior (constant k_c) is $R_g = 10$ μm.

The simple shrinking core model assumes the NiO grain or particle is non-porous, and Eq. (5) applies only under these circumstances. For example, Sridhar et al. [25] studied the reduction of NiO particles calcined at 1000 °C and presumably non-porous. These authors found satisfactory fits to Eq. (5) up to NiO con-

versions of 0.8, above which reduction became slower. They speculated that the increasingly thick (and perhaps dense) product layer made diffusion of water out of the particle more difficult.

Reduction of porous particles was addressed by Szekely and coworkers [26–29] and applied to experimental measurements on NiO [31]. These authors viewed the pellet or particle as a porous agglomeration of NiO grains each undergoing a microscopic shrinking core reduction. Depending on temperature, pellet size and porosity, asymptotic solutions reflect either chemical reaction control (low temperatures, small pellets, high porosities) or internal diffusion control (high temperatures, large spheres, low porosities, towards the end of the reaction). For the first case, the reaction proceeds uniformly throughout the pellet, with each grain undergoing the same shrinking core kinetics, unless there is a distribution of grain sizes. For the second, there exists a sharp reaction front or interface in the pellet that moves progressively towards the center. Predictions for mixed control show a diffuse front moving inward. The most serious restriction of the model is the requirement that the pellet maintain its structure, i.e. the individual grains retain approximately the same size and location as NiO converts to Ni. Since the model is empirical without analytical solutions, it has not been a convenient tool for kinetic interpretation.

In studies of NiO reduction Richardson et al. conducted at series of experiments using isothermal H_2 consumption and magnetization measurements to determine the Ni–O bond rupture (NiO conversion) and the growth of nucleated Ni^0 atoms (Ni growth), respectively [32]. They found the growth process lagged NiO conversion by a time interval that increased with decreasing temperature, lower gas flow rates and the presence of H_2O added to the reducing gas. They suggested that adsorbed H_2O molecules, produced by the reaction or added to the reducing gas, retard the growth process by limiting diffusion of Ni^0 atoms to appropriate nucleation centers. However, since the H_2 consumption and magnetization measurements were separate experiments, both using small packed beds of NiO grains, there was some concern that the observed "lag" could be an experimental artifact.

In this paper, we report the results of a NiO reduction study using a technique that avoids this objection: in situ hot-stage X-ray diffraction (XRD) that

measures NiO loss and Ni appearance simultaneously. Together with the ability to provide NiO and Ni crystallite sizes during reduction, this method uses a thin slab sample geometry that avoids problems inherent to packed beds.

2. Experimental

2.1. Sample preparation

The sample of NiO was prepared from high purity $Ni(NO_3)_2 \cdot 6H_2O$ solution by coprecipitation with 4 N Na_2CO_3 solution. The gel so formed was washed with deionized water until the filtrate was free of nitrate ion, with the remaining solid dried in air at 110 °C and calcined in air at 300 °C. Properties of the final product are given in Table 1.

2.2. Hot-stage X-ray diffraction

The principal technique used in this study was high temperature XRD, using a Siemens D 5000 diffractometer, equipped with a Huber germanium incident-beam focusing monochromator, a Buhler high-temperature stage, and a Braun position sensitive detector (PSD). The system was interfaced with a digital MicroVAXII computer, which was part of a

Table 1
Properties of the NiO sample [32]

Particle size (μm)	10–20
Color	Black
Stoichiometry	$NiO_{1.019}$
Surface area ($m^2\,g^{-1}$)	253
Crystallite size (nm)	
d_{XRD}	4.3
$d_{magnetic}$	2.9
d_{BET}	3.4

larger cluster of network-interconnected VAX computers running the operating system. A copper-anode, 1.5 kW X-ray tube, followed by a monochromator, delivered a beam of Cu $K\alpha_1$ radiation (0.154051 nm) with only a 10% loss of intensity. This provided diffraction patterns with low background and high resolution, free from reflections due to Cu $K\alpha_2$.

Fig. 2 shows a schematic of the Bühler HDK 2.3 in situ hot-stage unit, comprising a water-cooled, vacuum tight, stainless steel chamber (diameter: 10 cm, internal volume: 850 cm^3) with a beryllium window covering 165°. Most of the internal fittings were mounted on the front flange, which was inserted into the rear part of chamber attached to the goniometer. Fig. 2 shows only those features relating to the performance of the device.
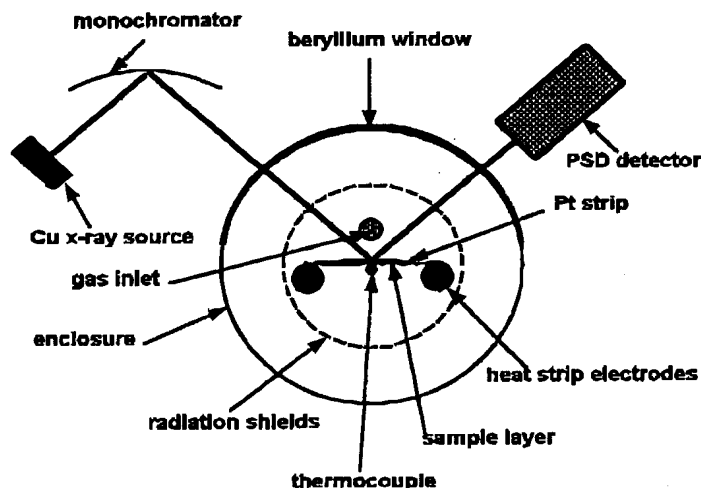

Fig. 2. Schematic of hot-stage XRD chamber.

The heating strip was a length of 90% Pt/10% Rh alloy tape (Johnston Matthey, 0.23 mm thick) mounted on two water-cooled, stainless steel electrodes. One was stationary and the other could be rotated from the outside to produce tension in the strip to ensure the tape was flat during heating. This tension was maintained during heating with a spring arrangement on the outside. The sample was applied as a porous layer to the Pt–Rh strip, which was heated with a LET 2401 power supply delivering up to 100 A at 8.5 V. Temperatures of up to 1600 °C were possible with this arrangement. The sample temperature was measured and the power supply controlled with a thin type S (Pt–Pt/10% Rh) thermocouple spot-welded to the strip close to the sample and isolated from the power supply with an Analog Devices 2B50B signal conditioner. This thermocouple was calibrated using a series of temperature standards with well-defined phase transitions.

The heating strip was surrounded with concentric thermal radiation shields to reduce heat losses to the chamber walls and prevent temperature gradients in the sample. Also, an environmental heater, with openings for the X-ray beam, was wrapped around the electrode-sample assembly and heated by two other electrodes (not shown). The controller maintained this heater at slightly lower temperatures than the strip.

Flow of reaction and purge gases (H_2, N_2) though the chamber was regulated with Tylan mass flow controllers using an external mixing manifold. Tubing and fittings were made of 316 stainless steel and Swagelok Instrumentation Quick-Connects. A stainless steel tube was interwoven through the radiation shields and emerged close to the sample, so that inlet gases entered behind the shield and provided a constant vapor composition in the reactor. Typically, flows of 200 cm³ min⁻¹ were used.

For runs involving added water, the reducing gas (20% H_2 in N_2) was humidified with a saturator comprising a sparged bubbler maintained at a sub-ambient temperature to ensure no moisture condensed in the X-ray apparatus. The system was large enough to achieve greater than 99.9% saturation at the regulated temperature. For example, with the saturator at 19 °C, the corresponding value of P_w was 2.2×10^{-2} atm.

During operation, the monochromatic X-ray beam entered the chamber though the beryllium window and was diffracted by the sample into the oscillating PSD. This PSD consisted of a 20-μm straight Pt wire ap-proximately 50 mm in length. Electrical impulses created by X-ray photons striking along the wire were translated into angle position and intensity. The PSD collected X-ray photons over an angular range (typically 5.25° (2θ)), with a very rapid data rate, and could be operated in both a continuous scanning mode, to obtain complete XRD patterns before and after reduction experiments, and a fixed mode, to follow rapid reactions through changes in a narrow range of less than 5.25° (2θ).

2.3. Experimental procedure

The NiO sample was ground in an agate mortar to a particle size of 10–20 μm, slurried with ethanol and about 20 mg applied to the Pt–Rh alloy strip using an artist's airbrush. The ethanol was evaporated under an infrared lamp, leaving a uniform coating with a thickness of about 50 μm. It was found initially that residual ethanol in the sample resulted in an induction period during reduction. This was eliminated by adopting a standard conditioning procedure as follows.

(1) After insertion of the sample holder, the chamber was treated at room temperature for 1 h with 160 cm³ min⁻¹ of N_2 at a pressure of 6 Torr.
(2) The catalyst was heated to 250 °C for 1 h in the N_2 flow at one atmosphere pressure.
(3) The chamber was flushed with 200 cm³ min⁻¹ of the reducing gas (20% H_2 in N_2) for one hour at ambient temperature and pressure.
(4) The temperature of the sample was increased (with the reducing gas flowing) to the reduction temperature with a heating rate of 20 °C s⁻¹, i.e. a maximum of about 15 s for the range 175–300 °C used in this study.

The objective was to measure the disappearance of NiO and the simultaneous appearance of Ni during reduction with as much precision as possible. For this purpose, the XRD peaks for NiO and Ni used for analyses must be located within 5.25° 2θ from each other to utilize the most precise fixed scan mode of the PSD detector. Table 2 lists the dominant peaks of NiO and Ni available in this range [33]. There were two possibilities: NiO, 43.29° (2θ); Ni, 44.50° (2θ); and NiO, 75.42° (2θ); Ni, 76.39° (2θ), and we selected the first pair since they are the most intense. A minimum scan time of 30 s was necessary, since a resolution 0.02°

Table 2
XRD peaks for NiO and Ni [33]

2θ	$[h\,k\,l]$	I/I_0
NiO		
37.26	1 1 1	63
43.29	2 0 0	100
62.88	2 2 0	48
75.42	3 1 1	17
79.41	2 2 2	12
Ni		
44.50	1 1 1	100
51.86	2 0 0	44
76.39	2 2 0	19

(2θ) was needed to deconvolute the peaks from 40 to 45° (2θ). The shortest practical reaction time was 10 min for a series of 27 equally spaced scans over the complete reduction period.

With the reducing gas flowing, the temperature was raised to the reaction temperature and measurements taken over the 40–45° (2θ) scan at frequent intervals until the reaction was complete. Typical results are shown in Fig. 3 for a partially reduced sample at about 10% NiO conversion. The target NiO[2 0 0] peak is so broad, due to small crystallite size, that it is partly beyond the scanning range and a section of the NiO[1 1 1] is included. Nevertheless, it was possible to deconvulute the peaks with appropriate software so that NiO[2 0 0] and Ni[1 1 1] peak intensities could be determined with a precision of ±2%. This procedure was followed for 27 scans in the run, and NiO and Ni conversions calculated by normalizing the areas with
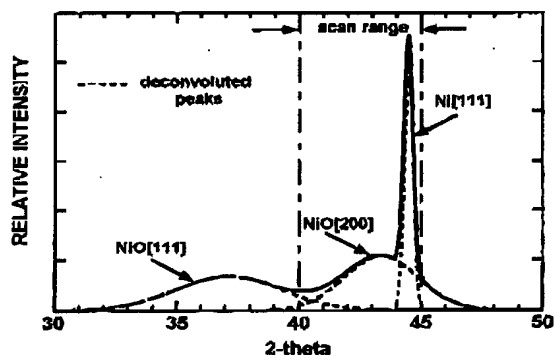

Fig. 3. XRD scan for NiO and Ni peaks for about 10% reduction at 175 °C.

the initial and final NiO and Ni areas, respectively. This assumed that reduction was complete at the end of the run, an assumption that was confirmed by heating the final sample to 500 °C in helium and running a complete ambient temperature XRD scan of the sintered (and sharpened) peaks.

There was some concern during the preliminary experiments that the Pt–Rh heating strip could influence the reduction by dissociating H_2 and initiating the reaction, especially at lower temperatures. This was checked by using a gold-plated Pt–Rh strip for selected experiments in the 175–300 °C range. Reduction curves were obtained that were identical to those with the non-plated strip, within experimental error. We concluded that any effect of the Pt–Re on the reduction mechanism was too small to be detected, and the non-plated strip was used thereafter.

2.4. Crystallite size measurement

Crystallite sizes of NiO and Ni were measured using the peak width at half peak height, β, in the Debye–Sherrer equation:

$$d_{XRD} = \frac{0.89\lambda}{(\beta - \beta_0)\cos\theta} \tag{6}$$

where d_{XRD} is the volume average diameter of the crystallite, λ the Cu Kα_1 wavelength, and β_0 the instrumental line broadening found experimentally from sintered NiO and Ni samples (0.188° (2θ) for NiO and 0.148° (2θ) for Ni). This procedure, in which only one peak was used, gave only a lower limit to the size, since there was no opportunity for a more detailed analysis using several peaks to find the broadening contribution from microstrain, as described by Williamson and Hall [34].

2.5. Thermogravimetric analysis

Weight loss during reduction was determined with a Seiko Instruments TG/DTA 320 thermogravimetric analyzer. About 5 μg of sample was degassed by heating in N_2 at 100 °C and then reduced in a 20% H_2/N_2 mixture at a total flow rate of 243 cm^3 min^{-1} and heating rates from 1 to 20 °C min^{-1}. The objective of these runs was to confirm complete reduction and to find the activation energy for reduction, E, from analysis of the variation of the temperature for the maximum

reduction rate, T_m, with heating rate. This was done using Eq. (7):

$$\ln\left(\frac{\alpha}{T_m^2}\right) = -\frac{E}{RT_m} + \ln\left(\frac{Rk_0}{E}\right) \quad (7)$$

where α is the heating rate, R the gas constant, E the activation energy and k_0 is the pre-exponential factor in the Arrhenius equation [35].

3. Results and discussion

3.1. Kinetics of reduction

Fig. 4 shows typical results for NiO reduction at 175 °C. There was a slight induction period, followed by a steady decrease in NiO concentration and a corresponding increase in Ni concentration. It is significant that metallic Ni was observed simultaneously with NiO loss, indicating that nucleation of Ni species and subsequent growth into crystallites was very fast, even at this relatively low temperature. This was contrary to previous observations using H_2 consumption and magnetization measurements [32]. This correspondence between NiO loss and Ni generation was observed in all reduction runs, so that kinetic analysis should give the same results. In this series of experiments, we only report results for the disappearance or loss of NiO.

Attempts were made to fit the loss of NiO data over the complete conversion range with suitable rate expressions derived from existing models for reduction, including diffusional effects [15]. Fifteen different rate
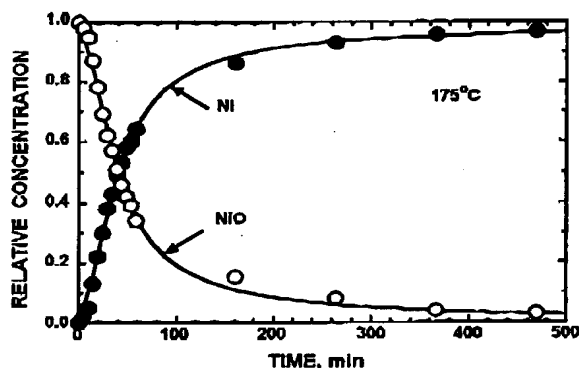
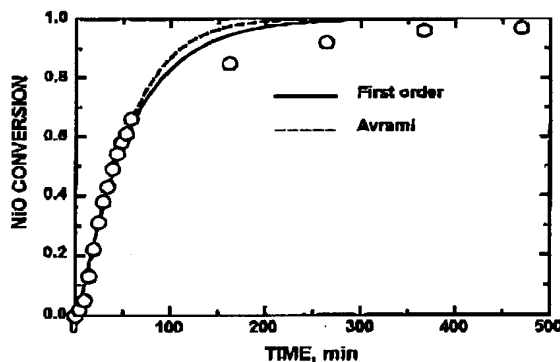Fig. 4. NiO disappearance and Ni appearance at 175 °C.

Fig. 5. First-order and Avrami kinetics for NiO reduced at 175 °C.

equations were identified and tested, but none gave satisfactory and consistent results over the range of temperatures from 175 to 300 °C, with the exception of the first-order and Avrami models. Fig. 5 demonstrates this for NiO data at 175 °C. Eq. (3) was used for the Avrami fit ($m = 1.23$) and Eq. (8) for first order:

$$x_{NiO} = 1 - e^{-k(t-t_0)} \quad (8)$$

where t_0 is a correction for any induction period. Since the first-order model is more consistent with a chemical reaction and rapid nucleation, we adopted the procedure of fitting the data with first-order kinetics up to conversion levels from 0.7 to 0.8, and this is the curve shown in Fig. 5. We believe that departure from first-order kinetics at higher conversions reflects a change in mechanism in which either NiO crystallites become less accessible, possibly as they are surrounded by Ni metal or densification around NiO crystallites inhibits water removal.

The effect of reduction temperature on NiO conversion is shown in Fig. 6 over the temperature range 175–300 °C. An induction period at 175 °C is evident, but it disappeared at higher temperatures. Also, reduction retardation at higher conversions is not present above 250 °C.

It has been known for many years that water vapor added to the reducing gas retards NiO reduction, and this is seen clearly in Fig. 7, which also shows the details of the early part of the reduction. Reduction at 250 °C without added water shows no induction effect, whereas reduction in the presence of 2.2×10^{-2} atm of added water slowed the reduction rate and exhibited
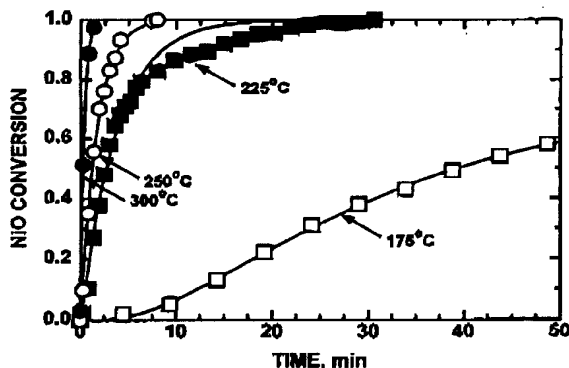
Fig. 6. Reduction of NiO in the temperature range 175–300 °C.

Fig. 8. Arrhenius plots for NiO reduction with and without added water.

the beginning of an induction period. At 225 °C, there was the suggestion of induction even without water, but a pronounced induction period was observed with added water as the rate decreased more dramatically. Clearly, water molecules on the surface increase the induction period and decrease the reduction rate, with the effects less significant at higher temperatures.

Fig. 8 shows the Arrhenius dependence of NiO reduction, with and without added water. For dry reduction, the apparent activation energy, E, is $85 \pm 6 \, kJ \, mol^{-1}$ and the pre-exponential constant ($k_0 P_H$), is $(1.88 \pm 0.13) \times 10^8 \, min^{-1}$, increasing to $126 \pm$
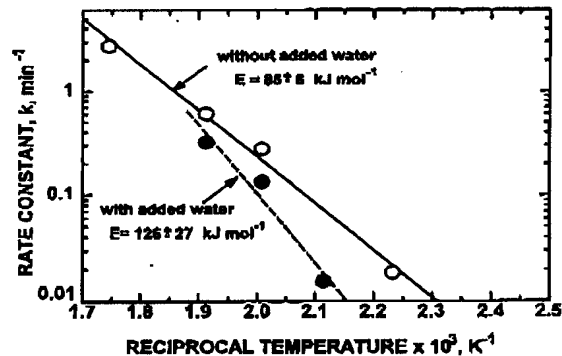
$27 \, kJ \, mol^{-1}$ and $(1.40 \pm 0.33) \times 10^{12} \, min^{-1}$, respectively, in the presence of water.

3.2. NiO and Ni crystallite sizes

The NiO crystallite size, d_{XRD}, decreased during reduction from an initial value of 2.7 nm to final values below 0.9 nm, at which point the XRD lines were so broad that accurate estimates of size were not possible (Fig. 9). The significant result was the large size of the resulting Ni crystallites, which increased by a factor of about 10–20 larger than the NiO at increasing
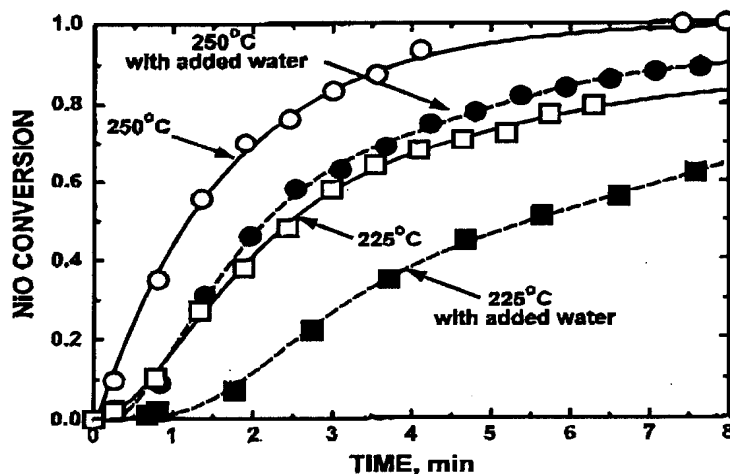

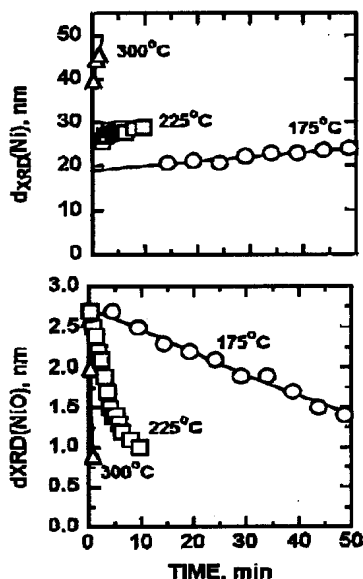Fig. 7. Effect of added water on the reduction of NiO at 225 and 250 °C.

Fig. 9. Crystallite sizes of Ni (upper) and NiO (lower) during reduction.

Fig. 11. Effect of added water on the NiO crystallite volume during reduction at 225 °C.

temperatures. Clearly, Ni crystallites formed from NiO reduction rapidly agglomerate and sinter.

Some insight into the reduction process is gained from Fig. 10 in which NiO crystallite volumes are plotted against conversions. For the shrinking core model, a linear decrease to zero at full conversion is expected. The results for 225–300 °C reduction are lower than predicted by the shrinking core model. At 175 °C, with 20% of the NiO reduced, the average crystal-
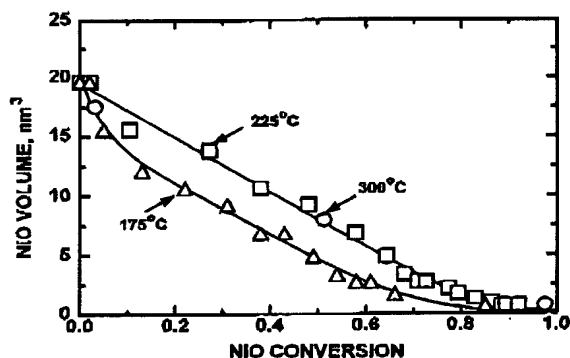
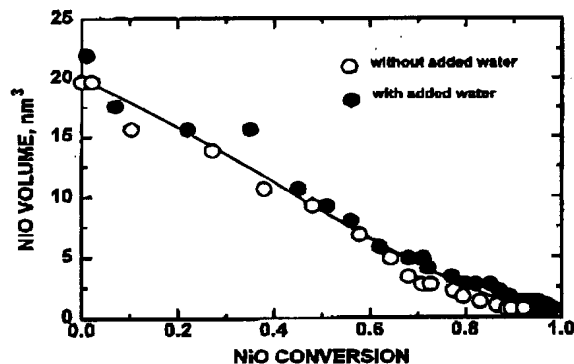lite volume was reduced by almost one half, implying the biggest loss occurred for larger crystallites. Presumably, there may have been a distribution of sizes with the larger crystallites reducing faster. The effect was less significant as temperature increased, so that a shrinking core model may be appropriate at some point. There was no significant difference between the curves for NiO at 225 °C, with and without water vapor in the reducing gas (Fig. 11), suggesting the effect is not dependent on NiO crystallite size.

3.3. TGA results

The TGA results (Fig. 12) indicated a slow reduction until 275 °C, at which point an accelerated loss of weight occurred until complete reduction was
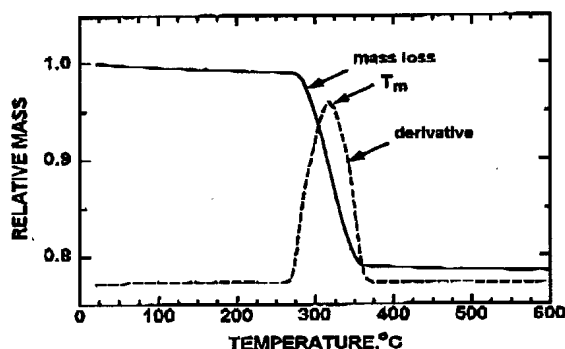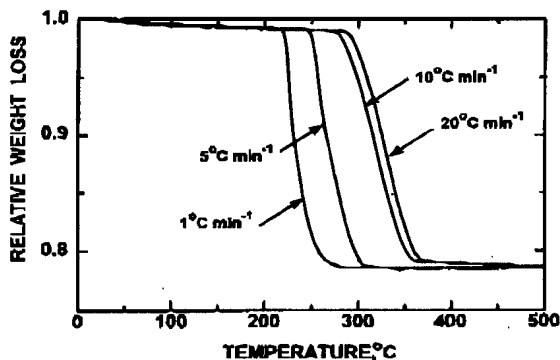

Fig. 10. NiO crystallite volumes during reduction.

Fig. 12. TGA data for NiO reduction at $10°$ min^{-1}.

Fig. 13. Effect of heating rate on TGA data for NiO reduction.

Fig. 14. Activation energy of reduction from TGA data.

achieved at 350 °C. The value of T_m or the peak maximum was determined from the derivative of the weight loss curve. Fig. 13 demonstrates the effect of increasing heating rate, and Fig. 14 is based on Eq. (7), from which $84 \pm 14 \, kJ \, mol^{-1}$ for E and $(2.31 \pm 0.9) \times 10^7 \, min^{-1}$ for $(k_0 P_H)$ were derived. The value of E is very close to $85 \pm 6 \, kJ \, mol^{-1}$ found from XRD measurements, but $(k_0 P_H)$ is about a factor of 10 smaller than the previously observed $(1.88 \pm 0.13) \times 10^8 \, min^{-1}$. This discrepancy is understandable, since acceptable activation energies
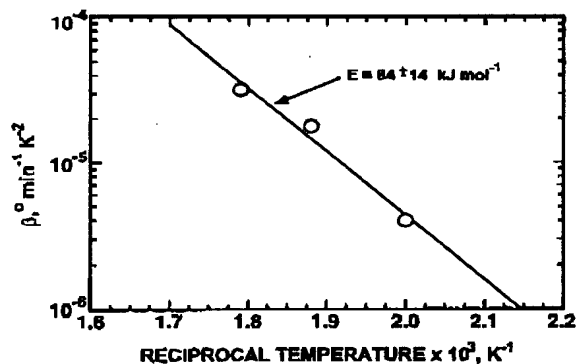
result from most models based on non-isothermal, programmed thermal methods, while pre-exponential constants often depend upon the assumptions of the model [35].

3.4. Activation energies

Reduction activation energies, reported by many researchers (Table 3), vary considerably from 17 to $133 \, kJ \, mol^{-1}$, depending upon conditions. The values fall into four groups. The first group exhibits activation

Table 3
Activation energies for the reduction of pure NiO by H_2

Source	Experimental procedure	Temperature range (°C)	E (kJ mol^{-1})
Szekely and Evans [27]	Thermobalance, large porous single pellet	372–753	17
Sridhar et al. [25]	Thermobalance, non-porous powder	291–509	18
Deb Roy and Abraham [36]	Thermobalance, non-porous spherical pellets	400–800	22
Szekely et al. [31]	Thermobalance, pressed cylinder	259–308	44
Chiesa and Rigaud [37]		250–300	47
Delmon and Roman [14]	Thermobalance, thick slab	215–260	50
Bandrowski et al. [19]	H_2O detection, large porous pellets large packed bed	261–298	52
Szekely and Evans [29]	Thermobalance, large porous pellet	226–308	65
Nakajima et al. [38]	Powdered sample	277–377	69
This study	TGA, porous powder, basket	220–355	84
This study	XRD, porous powder, thin slab	175–300	85
Nakajima et al. [38]	Thermobalance, thick slab	177–267	98
Parravano [9]	Thermobalance, thick slab	155–200	110
Chiesa and Rigaud [37]	Thermobalance, pellets	180–250	110
Rozhdestvenskii et al. [39]	Thermobalance, pellets	283–352	111
Charcosset et al. [12]	Thermobalance, thick slab	About 220	120
This study	XRD, porous powder, thin slab with water added	175–250	126
Richardson et al. [32]	H_2 consumption, porous powder packed bed	210–310	127
Szekely et al. [31]	Thermobalance, pressed thin disc	224–259	133

energies from 17 to 22 kJ mol⁻¹, a very low value that is more indicative of external or very strong pore diffusional than chemical resistance. The experimental conditions used support this conclusion; temperatures are very high and very large porous pellets were used or the powder was non-porous with a large grain size.

The temperature range in the second group is moderate, with activation energies of 44–52 kJ mol⁻¹, found with large porous pellets or slab-like samples. Activation energies are approximately one-half of the third group, suggesting that pore diffusion of some type is controlling the reduction. The third group, with values from 65 to 98 kJ mol⁻¹ were obtained from experiments with small-grain powders in loosely packed samples or thin slabs and is more suggestive of chemical control. Specifically, this group includes results from this study that were obtained under the most favorable conditions for chemical control.

The fourth group covers the same temperature range as the third but exhibits activation energies from 98 to 133 kJ mol⁻¹. Since the group includes results from this study in which water was added, a possible explanation for the higher activation energy is retention of H_2O molecules on the surface due to the presence of thick samples or packed beds in which removal of water of reaction from the sample is retarded. Richardson et al. suggested that such a mechanism prevails for supported $NiO/\alpha-Al_2O_3$ catalysts and a similar situation may apply here [32]. Bandrowski et al. [19] believed that, if the surface coverage of H_2O is high, then Eq. (4) becomes

$$-r_{NiO} = \left(\frac{k}{K_w P_w}\right) C_{NiO} P_H \qquad (9)$$

and the apparent activation energy, E_{app}, is given by

$$E_{app} = E - \Delta H_w \qquad (10)$$

where ΔH_w is the enthalpy of water adsorption on NiO. Since this is always exothermic (i.e. ΔH_w is negative), the observed activation energy increases when water retards the reduction. Using our results for the activation energies with and without added water yields $\Delta H_w = 41$ kJ mol⁻¹. However, Bandrowski et al. [19] found that K_w is 3.3 atm⁻¹ at 295 °C. This is not enough to ensure that $K_w P_w \gg 1$, which is a necessary condition for Eq. (9). We conclude that the increased activation energy with added water is not
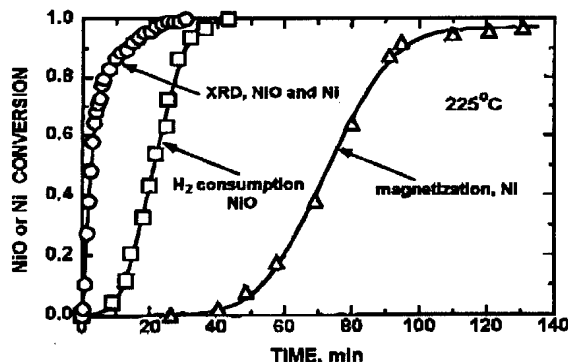

Fig. 15. Comparison of different techniques for NiO reduction.

due to a Langmuir–Hinshelwood term but reflects an increased barrier to the overall reduction mechanism.

3.5. Comparison of techniques

In previous research, we reported kinetic measurements on this NiO sample at close to 225 °C, using H_2 consumption to track the disappearance of NiO and magnetization measurements to determine Ni metal growth [32]. These past results are reproduced and compared to the present XRD data in Fig. 15. There are profound differences. The XRD data showed very rapid reduction of NiO and the simultaneous appearance of Ni. Hydrogen consumption was much slower with a pronounced induction period. Magnetization measurements indicated a retardation of Ni crystallite growth, with an extremely long induction period, implying that nucleation of Ni atoms lags the reaction with H_2. It is significant that magnetization measurements were made in a separate apparatus with repeated heating and cooling of the sample at each data point. This may have introduced some errors, but probably not enough to account for the large lag of 300 min at 220 °C.

The greatest difference between the three techniques used to study NiO reduction was sample geometry. Hydrogen consumption and magnetic sample tubes (4 mm diameter, 5.2 mm length and 3.08 mm diameter, 7 mm length, respectively) were cylindrical packed beds of fine grains. Both experiments were run at reducing gas flow rates of 150 cm³ min⁻¹, so the average partial pressures of water vapor in the

beds originating from reduction was $4–5 \times 10^{-2}$ atm. In contrast, the average partial pressure of water in the XRD experiment (without added water) was 3.5×10^{-3} atm. The results in Fig. 15 suggest that H_2 consumption is retarded but Ni nucleation is slowed even more for the higher water partial pressure prevailing in the packed beds. This is consistent with the activation energy for H_2 consumption in Table 3, which is $126 \, kJ \, mol^{-1}$, i.e. in the range of water retardation. Similarly, when water was added to the XRD runs, the activation energy was $127 \, kJ \, mol^{-1}$ and the rate was retarded (Fig. 7). However, Ni formation does not lag NiO reduction, which suggests evolution of water molecules from the surface is slower in the packed beds than in the slab (XRD) sample.

3.6. Model for reduction of NiO

The average grain size of the NiO powder examined in the present experiments was 20 μm, with crystallites about 3 nm in size. This means there are approximately 3×10^{11} crystallites in the grain, which is very porous with a BET surface area of $253 \, m^2 \, g^{-1}$. The system falls into the category described by Szekely and coworkers [26–31] as a porous particle with uniform reduction throughout but with a shrinking core for each reducing entity. However, the NiO crystallite diameters are below the critical size of 10 μm that Delmon and Pouchot found necessary for shrinking core behavior [24]. This is consistent with the results of Richardson and Twigg, who conducted temperature programmed reduction measurements on NiO powders with crystallites ranging from 7 to 163 nm in size and found that temperatures necessary for 0.5 conversion were almost constant [40]. This indicates that, for NiO crystallites this small, the rate of reduction is independent of diameter and stoichiometry, since the two are related [41]. Furthermore, as NiO crystallites reduce, Ni crystallites almost ten times as large quickly form, each containing Ni atoms from about 300 NiO crystallites. Clearly, this does not conform to the Szekely model, since constant structural geometry is not maintained.

Reduction of bulk NiO reported here follows the mechanism described by Benton and Emmett 75 years ago [5] and supported by many researchers since then. Hydrogen quickly diffuses throughout the grain and reacts with NiO forming Ni^0 atoms and

H_2O. Rodriguez et al. have reported experiments in which the induction process was investigated with X-ray absorption fine structure, photo-emission and synchrotron-based time-resolved XRD, supported with density-function slab calculations [42]. These authors concluded that, in order for H_2 to dissociate on NiO, H_2 must react with two Ni atoms separated by an oxygen lattice vacancy. Since NiO crystallites, as prepared here, contain excess oxygen, the induction period commonly observed could be due to slow generation of these vacancies as reducing gas sweeps over the sample and removes excess oxygen. This effect is expected to be slower at lower temperatures, where induction periods are most often observed.

Once liberated, Ni atoms nucleate into metallic clusters that grow in size until they are large enough to initiate H_2 dissociation, at which point the reduction process accelerates autocatalytically. This induction period is longer at lower temperature and in the presence of adsorbed water molecules originating from the reaction or water vapor added to the reducing gas.

Reduction proceeds with pseudo-first-order kinetics if H_2 is in excess, otherwise the rate is proportional to H_2 pressure and NiO concentration. Added amounts of H_2O on the surface (either incipient or added) retards this step, with a decreasing effect at higher temperatures. This implies that reduction rates could be enhanced by removing the water of reaction as soon as it forms. Higher temperatures favor rapid water removal, but at lower temperatures the water molecules strongly adhere to the surface and are further constrained by transport through the pores of the grain and within the bed structure of the sample. Thin, slab-like samples are a close as possible to achieving accelerated egress of the water, but adsorptive forces still exert an influence. Possibly, reduction at lower pressures could achieve a further improvement in reduction rate.

Nickel oxide crystallites decrease in size in a manner suggestive of a shrinking core, but since the rate is constant with size, i.e. not proportional to the interfacial area, predicted shrinking core kinetics are not observed. Nickel clusters rapidly agglomerate into metallic nickel crystallites due to the small distances between NiO crystallites in bulk NiO. These Ni crystallites are over ten times as large as the NiO crystallites, and growth kinetics mirrors NiO disappearance. The NiO grain transforms into an agglomeration of Ni crystallites decorated with smaller NiO crystallites.

Ultimately, the NiO crystallites become less accessible and the reduction rate slows, most probably due to the difficulty of H_2O molecules escaping from the NiO surface through the surrounding layer of metal.

The Ni growth process also slows if high concentrations of H_2O exist in the pores of the NiO. In samples comprising a packed bed of grains, the effect is dramatic. Nickel growth, as detected by magnetic measurements, lagged NiO dissociation by an amount that increased at lower temperatures. However, this was not observed with XRD measurements, where the sample consisted of well-dispersed grains. Water inhibition of metal growth is apparently very sensitive to sample morphology.

The significant feature in this mechanism is rapid diffusion of Ni^0 atoms away from the reducing NiO surface. With bulk NiO, there is sufficient contact between neighboring NiO crystallites to promote this transport. This situation does not prevail in supported NiO catalysts, where NiO crystallites are sufficiently separated that diffusion of Ni across the support surface is influenced by many factors, such as adsorbed H_2O and promoters. We have applied the same experimental techniques reported here to supported NiO catalysts, and the results of this work will be reported in a subsequent paper.

4. Conclusions

This research has demonstrated that in situ hot-stage XRD is an effective tool to study the chemical reduction of catalysts such as NiO. Sample topology may then be separated from morphology. Combinations between these two features have clouded the results from many other techniques, such as isothermal measurement of H_2 consumption, water generation, or magnetization. When applied to porous bulk NiO powder, the technique has revealed that NiO disappearance and Ni appearance is simultaneous, but the Ni crystallite size is about ten times larger than that of the original NiO. After a small induction period, the kinetics are pseudo-first-order up to conversions levels of about 0.8, when inaccessibility of NiO crystallites retards the rate. This is believed to be caused by retention of product H_2O on the surface and is substantiated by experiments in which water vapor added to the reducing gas at temperatures from 175 to 250 °C increased

the induction period and decreased the reduction rate, thus re-enforcing previous observations that the texture and morphology of the sample has a significant effect that complicates interpretation of NiO reduction kinetics. Micro-shrinking core models for the reduction of grains comprising small NiO crystallites do not apply.

Acknowledgements

References

[1] O. Antoin, L. Holappa, P. Paschen, Miner. Proc. Extr. Metal. Rev. 15 (1995) 169.
[2] D.E. Ridler, M.V. Twigg, in: M.V. Twigg (Ed.), Catalyst Handbook, Second ed., Wolfe Publishing Ltd., London, 1996, p. 225.
[3] A. Baranski, A. Koturba, J.M. Lagan, A. Pattek-Janczyk, E. Pyrczak, A. Reizer, Appl. Catal. A: Gen. 112 (1994) 13.
[4] D.R. Goodman, in: M.V. Twigg (Ed.), Catalyst Handbook, Second ed., Wolfe Publishing Ltd., London, 1996, p. 161.
[5] A.F. Benton, P.H. Emmett, J. Am. Chem. Soc. 46 (1924) 2728.
[6] G.B. Taylor, H.W. Starkweather, J. Am. Chem. Soc. 52 (1930) 2314.
[7] V.V. Boldyrev, M. Bulens, B. Delmon, The Control of the Reactivity of Solids, Elsevier, Amsterdam, 1979.
[8] K. Hauffe, A. Rahmel, Z. Phys. Chem. Frankfurt 1 (1954) 104.
[9] G. Parravano, J. Am. Chem. Soc. 74 (1952) 1194.
[10] A. Yamaguchi, J. Moriyama, J. Jpn. Inst. Metals 29 (1965) 831.
[11] H. Charcosset, R. Frety, A. Soldat, Y. Trambouze, J. Catal. 22 (1971) 204.
[12] H. Charcosset, R. Frety, G. Labbe, Y. Trambouze, J. Catal. 35 (1974) 92.
[13] J.T. Richardson, B. Turk, M. Lei, K. Forster, M.V. Twigg, Appl. Catal. A: Gen. 83 (1992) 87.
[14] B. Delmon, A. Roman, J. Chem. Soc., Faraday Trans. 1 69 (1973) 941.
[15] Y. Koga, L.G. Harrison, in: C.H. Bamford, C.F.H. Tipper, R.G. Compton (Eds.), Comprehensive Chemical Kinetics, vol. 21, Elsevier, Amsterdam, 1984, p. 120.
[16] M. Avrami, J. Chem. Phys. 7 (1939) 1103.
[17] M. Avrami, J. Chem. Phys. 8 (1940) 212.
[18] M. Avrami, J. Chem. Phys. 9 (1941) 177.

[19] J. Bandrowski, C.R. Bickling, K.H. Yang, O.A. Hougen,
     Chem. Eng. Sci. 17 (1962) 379.
[20] J. Moriyama, A. Yamaguchi, Nippon Kinzoku Gakkaishi 28
     (1964) 831.
[21] Y. Iida, K. Shimada, J. Chem. Soc. Jpn. 33 (1960) 1194.
[22] S. Yagi, D. Kunii, in: Proceedings of the 5th International
     Symposium on Combustion, Roinhold, New York, 1955,
     p. 231.
[23] B. Delmon, Introduction a la Cinetique Heterogene, Technip,
     Paris, 1969.
[24] B. Delmon, M.T. Pouchot, Bull. Soc. Chim. Fr. (1966) 2677.
[25] S. Sridhar, D. Sichen, S. Seetharaman, Z. Metallkd. 85 (1994)
     616.
[26] J. Szekely, J.W. Evans, Chem. Eng. Sci. 25 (1970) 2639.
[27] J. Szekely, J.W. Evans, Chem. Eng. Sci. 26 (1971) 1901.
[28] J. Szekely, J.W. Evans, Metal. Trans. 2 (1971) 1691.
[29] J. Szekely, J.W. Evans, Metal. Trans. 2 (1971) 1699.
[30] H.Y. Sohn, J. Szekely, Chem. Eng. Sci. 27 (1972) 763.
[31] J. Szekely, C.L. Lin, H.Y. Sohn, Chem. Eng. Sci. 28 (1973)
     1975.
[32] J.T. Richardson, M. Lei, B. Turk, K. Forster, M.V. Twigg,
     Appl. Catal. 110 (1994) 217.

[33] Powder Diffraction File, Joint Committee on Powder
     diffraction, International Center for Diffraction Data,
     Swarthmore, PA, 1987, Card. 4-0835.
[34] G.K. Williamson, W.H. Hall, Acta Metal. 1 (1953) 22.
[35] N.W. Hurst, S.J. Gentry, A. Jones, B.D. McNicol, Catal. Rev.
     Sci. Eng. 24 (1982) 233.
[36] T. Deb Roy, K.P. Abraham, in: J.H.E. Jeffes, R.J. Tait (Eds.),
     Physical Chemistry of Process Metallurgy; the Richardson
     Conference, Institute of Mineral Metallurgy, London, 1974,
     p. 85.
[37] F. Chiesa, M. Rigaud, Can. J. Chem. Eng. 49 (1971) 617.
[38] M. Nakajima, S. Shimizu, K. Onuki, Y. Ikezoe, S. Sato,
     Chem. Soc. Jpn. 4 (1989) 681.
[39] V.P. Rozhdestvenskii, L.M. Volgina, T.P. Strokova, Zh. Priki.
     Khim. 40 (1967) 705.
[40] J.T. Richardson, M.V. Twigg, J. Appl. Catal. A: Gen. 167
     (1998) 57.
[41] J.T. Richardson, D.I. Yiagas, B. Turk, K. Forster, M.V. Twigg,
     J. Appl. Phys. 70 (1991) 6977.
[42] J.A. Rodriguez, J.C. Hanson, A.I. Frenkel, J.Y. Kim, M.
     Perez, J. Am. Chem. Soc. 124 (2002) 346.